Pergamon

Int. J. Heat Mass Transfer. Vol. 39, No. 17, pp. 3595–3606, 1996

0017-9310/96 $15.00 + 0.00

PII: S0017-9310(96)00048-8

Wall-bounded buoyant turbulent flow and its modeling

T. P. SOMMER† and R. M. C. SO‡

Mechanical and Aerospace Engineering, Arizona State University, Tempe, AZ 85287-6106, U.S.A.

(*Received* 23 *August* 1995 *and in final form* 20 *January* 1996)

Abstract—A turbulent heat-flux model for buoyant flows is derived based on algebraic modeling techniques. Buoyancy terms are included in order to allow for the prediction of counter-gradient transport. The model incorporates a mixed time scale, based on both the velocity and thermal turbulence time scales and relaxes the assumption of a constant turbulent Prandtl number. Thus simplified, the algebraic equations, which are explicit in the heat fluxes, depend explicitly on buoyancy, the mean velocity and thermal fields, the turbulent kinetic energy and its dissipation rate and the temperature variance and its dissipation rate. Near-wall corrections are formulated to make the model asymptotically consistent as a wall is approached and this allows the heat flux equations to be integrated to the wall once the transport of the temperature variance and its dissipation rate and the velocity field are known. The nonbuoyant version of the model has been validated previously, therefore, the present model is applied to near-wall buoyant turbulent flows only. Test cases considered include fully developed horizontal channel flows with a heated bottom wall and turbulent flow in a heated vertical pipe. The prediction of both flow types by the present model are in agreement with experimental data. In view of these results, the present model is found to be capable of capturing the essential physics and yields asymptotically correct results near the wall for both buoyant and nonbuoyant incompressible turbulent flows.

INTRODUCTION

The necessity to model incompressible near-wall turbulent flows for a wide range of practical engineering problems has been recognized recently. Since then, a number of near-wall two-equation and second-order models have been proposed and validated against various turbulent flows [1, 2]. There are many engineering problems where buoyancy plays an important role. Different attempts to model buoyancy effects have been made in the past [3–14]. However, most of these efforts are not concerned with near-wall models; rather they concentrate on the modeling of buoyancy effects in a high-Reynolds-number medium. As a result, few studies have been carried out on near-wall buoyant turbulent flows.

In buoyant flow modeling, the Boussinesq hypothesis is usually invoked to simplify the governing equations. Even then, the uncoupled flow approximation [15] cannot be assumed. For nonbuoyant, nonisothermal incompressible flows, the temperature field is affected by the velocity model, but not the other way around. On the other hand, heat flux modeling has a significant effect on the overall calculations of buoyant turbulent flows. Consequently, a constant Pr_t assumption may not be very appropriate. This assumption is also inappropriate for incompressible, nonisothermal near-wall flows where Pr_t increases rapidly as the flow approaches the wall, depending on the thermal boundary conditions and the fluid Pr [16, 17]. In spite of this, numerous turbulence models invoking constant Pr_t have been proposed. Among the more representative work are the one-equation [3] and two-equation studies [4–7], where wall functions are used to link the properties at the first grid point to the wall. Since all these models invoke an eddy viscosity hypothesis for the Reynolds stress tensor $\overline{u_i u_j}$ and a constant Pr_t for the Reynolds heat flux vector $\overline{u_i\theta}$, they cannot predict counter-gradient heat transport. Furthermore, they do not allow for a variable time scale ratio R and the predictions are quite sensitive to the specific value chosen for Pr_t. These characteristics are important for the prediction of buoyant turbulent flows [9]. Another assumption that is very questionable in these models is the setting of $\overline{u\theta}$ equal to $\overline{v\theta}$ in order to obtain the correct sign for $\overline{u\theta}$ [8]. On the other hand, if Favre averaging [10] is adopted, the resulting model could be applied to cases with larger temperature variations, since a Boussinesq assumption is not necessary for the density field. However, it still suffers the same limitations as far as counter-gradient transport and R are concerned.

Several algebraic models derived with or without the use of a local equilibrium turbulence assumption have been proposed [8, 11–13]. In all but ref. [13], θ^2 is calculated from an equilibrium model with a constant R. On the other hand, the transport equations for θ^2 and ε_θ are solved in ref. [13]. These models are

† Present address: ABB Power Generation Ltd, Gas Turbine Development, CH-5401 Baden, Switzerland.

‡ Author to whom correspondence should be addressed. Present address: Mechanical Engineering, The Hong Kong Polytechnic University, Hung Hom, Kowloon, Hong Kong.

NOMENCLATURE

C_f skin friction coefficient
C_p specific heat at constant pressure
D pipe diameter
$\mathbf{D}_{ij}$ production tensor, $\mathbf{D}_{ij} = -\overline{\mathbf{u}_i\mathbf{u}_k}(\partial\bar{U}_k/\partial x_j) - \overline{\mathbf{u}_j\mathbf{u}_k}(\partial\bar{U}_k/\partial x_i)$
Gq Grashof number based on $\bar{q}_w$, $Gq = g\beta D^4\bar{q}_w/(\rho C_p\alpha\nu^2)$ or $Gq = g\beta H^4\bar{q}_w/(\rho C_p\alpha\nu^2)$
G generation/destruction of k due to buoyancy, $G = -g_i\beta\overline{\mathbf{u}_i\theta}$
G_{ij} generation/destruction of $\overline{\mathbf{u}_i\mathbf{u}_j}$ due to buoyancy, $G_{ij} = -g_i\beta\overline{\mathbf{u}_j\theta} - g_j\beta\overline{\mathbf{u}_i\theta}$
G_ε generation/destruction of ε due to buoyancy, $G_\varepsilon = -g_i\beta(\overline{\partial u_i/\partial x_k)(\partial\theta/\partial x_k)}$
g acceleration due to gravity
g_i ith component of gravity vector
H, h channel width and half width, respectively
k turbulent kinetic energy
Nu Nusselt number, $Nu = \bar{q}_w D(\Theta_w - \Theta_m)/(\rho C_p\alpha)$ or $Nu = \bar{q}_w H(\Theta_w - \Theta_m)/(\rho C_p\alpha)$
n_i ith component of the unit normal vector, positive outward from wall
p fluctuating pressure
$\tilde{P}$ production of k due to mean shear
Pr Prandtl number
P_{ij} production of Reynolds stresses due to mean shear
P_θ production of temperature variance, $P_\theta = -\overline{u_k\theta}(\partial\bar{\Theta}/\partial x_k)$
Pr_t turbulent Prandtl number
P_θ^* production of temperature variance due to streamwise mean temperature gradient
$\bar{q}_w$ mean wall heat flux
R time scale ratio, $R = (k/\varepsilon)/(\overline{\theta^2}/\varepsilon_\theta)$
Re Reynolds number based on bulk velocity, $Re = U_m D/\nu$ or $Re = U_m H/\nu$
Re_τ Reynolds number based on $\bar{u}_\tau$, $Re_\tau = \bar{u}_\tau h/\nu$ or $Re_\tau = \bar{u}_\tau R/\nu$
Re_t turbulent Reynolds number, $Re_t = k^2/(\nu\varepsilon)$
St Stanton number, $St = \bar{q}_w/\{\rho C_p U_m(\Theta_w - \Theta_m)\}$, $St = Nu/(RePr)$
$\bar{\mathbf{S}}_{ij}$ mean strain rate tensor, $\bar{\mathbf{S}}_{ij} = (1/2)(\partial\bar{U}_i/\partial x_j + \partial\bar{U}_j/\partial x_i)$
t time
U_m bulk mean velocity
$\bar{U}_i$ ith component of the Reynolds averaged velocity
$\bar{U}, \bar{V}, \bar{W}$ Reynolds averaged velocities along x-, y- and z-directions
U^+ mean velocity normalized with u_τ
u_i ith component of the fluctuating velocity
u, v, w Reynolds fluctuating velocities along x-, y- and z-directions
u_τ friction velocity, $u_\tau = \sqrt{\tau_w/\rho}$
$\bar{u}_\tau$ average friction velocity over hot and cold wall
$\overline{uv}^+$ normalized turbulent shear stress, $-\overline{uv}^+ = -\overline{uv}/u_\tau^2$
$\bar{\mathbf{W}}_{ij}$ mean rotation rate tensor, $\bar{\mathbf{W}}_{ij} = (1/2)(\partial\bar{U}_i/\partial x_j - \partial\bar{U}_j/\partial x_i)$
x_i ith component of the coordinate
x, y, z coordinates in streamwise, wall-normal and transverse directions
y^+ normalized wall-normal coordinate, $y^+ = yu_\tau/\nu$.

Greek symbols

α thermal diffusivity
α_t thermal eddy diffusivity
β coefficient of thermal expansion, $\beta = -(1/\rho)(\partial\rho/\partial\Theta)_p$
ε dissipation rate of k
ε_w ε at the wall, $\varepsilon_w = \nu(\partial^2 k/\partial y^2)_w$
$\tilde{\varepsilon}$ modified dissipation rate, $\tilde{\varepsilon} = \varepsilon - 2\nu(\partial\sqrt{k}/\partial y)^2$
$\bar{\varepsilon}$ modified dissipation rate, $\bar{\varepsilon} = \varepsilon - 2\nu k/y^2$
ε_θ dissipation rate of temperature variance
$\tilde{\varepsilon}_\theta$ modified dissipation rate of temperature variance, $\tilde{\varepsilon}_\theta = \varepsilon_\theta - \alpha(\partial\sqrt{\theta^2}/\partial y)^2$
ε_θ^* modified dissipation rate of temperature variance, $\varepsilon_\theta^* = \varepsilon_\theta - \alpha(\overline{\theta^2} - \overline{\theta_w^2})/y^2$
$\varepsilon_{\theta,w}$ ε_θ at the wall, $\varepsilon_\theta = (\alpha/2)(\partial^2\overline{\theta^2}/\partial y^2)_w$
$\varepsilon_{\theta i}$ dissipation rate of the heat flux vector $\overline{\mathbf{u}_i\theta}$
ν fluid kinematic velocity
ν_t eddy viscosity
$\bar{\rho}$ mean density
$\bar{\Theta}$ Reynolds averaged temperature
Θ_m bulk mean temperature
Θ_τ friction temperature, $\Theta_\tau = q_w/(\rho C_p u_\tau)$
θ Reynolds fluctuating temperature
$\overline{\theta^2}$ temperature variance
τ_w wall shear stress.

suitable for buoyant flows because they are able to replicate counter-gradient diffusive transport. Still, three of these models specify a constant R and invoke an equilibrium assumption to calculate θ^2. Furthermore, all but ref. [8] use wall functions to bridge the gap to the wall. The appropriate way to specify the wall functions for complex buoyant flows is not obvious at all. A further difficulty could arise in the algebraic models assumed for $\overline{u_i u_j}$. The matrix inversion of the system of algebraic equations could lead to numerical difficulties [18]. This is true even for models assuming local equilibrium turbulence, but can only get worse if this assumption is relaxed. On the other hand, Uspuras and Poskas [14] propose a full second-order model. They calculate $\overline{\theta^2}$ and ε_θ from their own transport equations, thus allowing for a variable R. The second-order model has not been widely tested and only sparse comparison with experiments is given by the authors. Furthermore, the approach using a full second-order closure is not very attractive because of the large numbers of equations involved. For a three-dimensional problem, the number of coupled partial differential equations to be solved consist of five mean flow equations, seven Reynolds-stress equations, five heat-flux equations plus an equation of state; thus givin a total of 18 equations. Therefore, it is important to seek simpler models that could correctly replicate the essential physics of wall-bounded buoyant flows.

It is clear from the above brief review that none of the models proposed to date are fully satisfactory when applied to calculate a wide variety of buoyant flows. The present objective is to propose a more general near-wall model for buoyant turbulent flows. It is based on a Reynolds-stress model for the velocity field and an explicit algebraic heat flux model for the temperature field. The latter model, which has been developed for near-wall nonbuoyant flows [19], will be modified with appropriate terms added to account for buoyancy effects. The additional buoyancy terms do not behave correctly in the near-wall region. Therefore, the near-wall corrections formulated for nonbuoyant flows have to be re-examined and modifications are derived to ensure asymptotic consistency near a wall. Furthermore, the heat-flux model is derived to allow an asymptotically correct behavior for $\overline{v\theta}$. The Reynolds-stress model is based on the nonbuoyant near-wall model of So *et al.* [20]. Since additional generation/destruction terms due to buoyancy appear explicitly in the equations, the pressure–strain correlation model [21] adopted has to be improved accordingly. The dissipation-rate equation is modified by including a buoyancy term to model a corresponding one appearing in the exact equation. Thus formulated, the modeled equations for $\overline{u_i u_j}$, ε, $\overline{\theta^2}$ and ε_θ, plus an explicit algebraic equation for $\overline{u_i\theta}$, form the basis of the present model.

The model is validated against benchmark flow cases. Wall-bounded buoyant flows could involve rather complicated physics, even though their geometry might be relatively simple. Petukhov and Polyakov [22] refer to the direct influence of buoyancy on the turbulence field as the structural effect and that on the mean field as the external effect. In developing vertical pipe flows with buoyancy influence, both effects appear at the same time. This is in contrast to horizontal channel flows with vertical stratification where only the structural effect is present. Since the two effects usually act in opposite directions, thus leading to opposite changes in parameters such as C_f, Nu and St, the resulting flow field is determined by a complicated interaction of structural and external effects [22]. It seems that most modeling studies discussed above consider flows where external effect is more important. Thus, model deficiencies are not easily revealed by these calculations. If, on the other hand, structural effect becomes more pronounced, then these deficiencies could hopefully become obvious immediately. In view of these differences, at least one of the test cases should involve structural effect alone.

NEAR-WALL MODIFICATIONS OF THE REYNOLDS-STRESS EQUATION FOR BUOYANT FLOWS

If the Boussinesq approximation is invoked for buoyant turbulent flow, the Reynolds-averaged equations for $\bar{U}_i$, $\overline{u_i u_j}$, ε, $\overline{u_i\theta}$, $\overline{\theta^2}$ and ε_θ can be reduced to a form similar to the incompressible equations with additional buoyancy terms appearing in the $\bar{U}_i$, $\overline{u_i u_j}$, ε and $\overline{u_i\theta}$ equations only [23]. The mean flow equations are coupled because of the presence of the extra buoyancy term. Also, the $\overline{\theta^2}$ equation needs to be solved, even if a second-order model is used to resolve $\overline{u_i\theta}$ because of the extra buoyancy term. For high-Re flows, the molecular diffusion terms can be neglected, but they should be retained for near-wall flows. According to Gebhart *et al.* [24], the Boussinesq approximation is valid if $R_0 = g\beta L/C_p \ll 1$, $R_1 = \Delta\rho/\bar{\rho} \ll 1$, $R_0 \ll R_1$ and there is no extreme variation of either R_1 or the reference density ρ_∞. These conditions are valid for a wide range of practical problems. The extra terms appearing in $\overline{u_i u_j}$, ε and $\overline{u_i\theta}$ are all exact within the framework of the Boussinesq approximation. However, it will be seen later that certain model terms also need to be modified to account for the buoyancy effects.

Near-wall nonbuoyant, incompressible flow modeling of $\overline{u_i u_j}$ using the high-Re proposals of Speziale *et al.* [21], Hanjalic and Launder [25] and Kolmogorov [26] for the pressure strain tensor, the turbulent diffusion tensor and the isotropic part of the dissipation rate tensor, respectively, has been reported previously [20]. The present approach modifies and extends this near-wall model to buoyant turbulent flows. According to Launder [23], an extra term due to buoyancy should appear in the pressure–strain tensor, which can be written symbolically as

$$\Pi_{ij} = \overline{\frac{p}{\bar{\rho}}\left(\frac{\partial u_i}{\partial x_j} + \frac{\partial u_j}{\partial x_i}\right)} = \Pi_{ij}^1 + \Pi_{ij}^2 + \Pi_{ij}^3. \qquad (1)$$

The first two terms are identical to those appearing in the nonbuoyant case and the model of [21] can be assumed for these terms. As for the third term, Launder [23] suggests relating it to the generation/destruction of $\overline{\mathbf{u}_i\mathbf{u}_j}$ due to buoyancy. The term proposed is

$$\mathbf{\Pi}_{ij}^3 = -C_6(G_{ij}-\tfrac{2}{3}\delta_{ij}G), \tag{2}$$

where $C_6 = 0.3$ is suggested. There is no need to add extra terms to account for the buoyancy effects explicitly in the turbulent diffusion and dissipation models [23]. Therefore, with equation (2) added to $\mathbf{\Pi}_{ij}$, the exact and the high-Re modeled $\overline{\mathbf{u}_i\mathbf{u}_j}$ equations can again be analyzed for asymptotic consistency following the procedure outlined in refs. [27, 28].

In the present approach, it is assumed that u, v, w and θ can be expressed as asymptotic series in terms of y, with the coefficients being random functions of t, x and z. Again, the wall temperature fluctuations are assumed to be zero. Although this assumption has only been tested for nonbuoyant flows [17], it could be expected to be valid for buoyant flows because, in the immediate vicinity of the wall, viscous effects are dominant, while buoyancy effects are not. Using these expansions, it can be shown that both the modeled and exact buoyancy generation terms are of higher order than the nonbuoyant terms and, thus, will not influence the near-wall balance of the equations. Even the buoyancy term $\mathbf{\Pi}_{ij}^3$ will only influence the near-wall balance in the $\overline{v^2}$-equation if and only if the gravity vector has a component parallel to the wall. In this case, the term is of order y^2, the same as the lowest order nonbuoyant term. If, on the other hand, the gravity vector is normal to the wall, this term is again of higher order. Therefore, it will not affect the near-wall balance of the $\overline{v^2}$-equation.

In previous heat transfer modeling studies [16], $\overline{u\theta}$ and $\overline{w\theta}$ are not modeled to the proper order so that additional wall damping functions could be avoided. This rationale is also applied to buoyant flow modeling. Thus, the modeling $\overline{u\theta}$ and $\overline{w\theta}$ would not be of order y^2, but of some higher order. Furthermore, the additional buoyancy term in the $\mathbf{\Pi}_{ij}$ model would also be of an order higher than y^2. In this case, even the near-wall balance of the $\overline{v^2}$-equation will not be influenced by the buoyancy terms and no near-wall correction to $\mathbf{\Pi}_{ij}^3$ is needed. Therefore, it is not necessary to introduce modifications to the near-wall corrections of the incompressible near-wall Reynolds-stress model [20], which can be summarized as

$$\frac{D\overline{\mathbf{u}_i\mathbf{u}_j}}{Dt} = \frac{\partial}{\partial x_k}\left(\nu\frac{\partial\overline{\mathbf{u}_i\mathbf{u}_j}}{\partial x_k}\right) + \mathbf{D}_{ij}^{\mathrm{T}} - \left(\overline{\mathbf{u}_i\mathbf{u}_k}\frac{\partial \bar{U}_j}{\partial x_k} + \overline{\mathbf{u}_j\mathbf{u}_k}\frac{\partial \bar{U}_i}{\partial x_k}\right) + \mathbf{\Pi}_{ij} - \varepsilon_{ij} + G_{ij}, \tag{3a}$$

$$\mathbf{D}_{ij}^{\mathrm{T}} = \frac{\partial}{\partial x_k}\left\{C_{\mathrm{s}}\frac{k}{\varepsilon}\left(\overline{\mathbf{u}_i\mathbf{u}_l}\frac{\partial\overline{\mathbf{u}_j\mathbf{u}_k}}{\partial x_l} + \overline{\mathbf{u}_j\mathbf{u}_l}\frac{\partial\overline{\mathbf{u}_k\mathbf{u}_i}}{\partial x_l} + \overline{\mathbf{u}_k\mathbf{u}_l}\frac{\partial\overline{\mathbf{u}_i\mathbf{u}_j}}{\partial x_l}\right)\right\}, \tag{3b}$$

$$\begin{aligned}\mathbf{\Pi}_{ij} = {} & -(2C_1\varepsilon + C_1^*\tilde{P})(1-f_{\mathrm{w1}})b_{ij} + C_2(1-f_{\mathrm{w1}}) \\ & \times \varepsilon(b_{ik}b_{kj} - \tfrac{1}{3}\delta_{ij}\Pi) - (\alpha_1 - \alpha^* f_{\mathrm{w1}})(P_{ij} - \delta_{ij}\tilde{P}) \\ & - \beta_1(\mathbf{D}_{ij} - \delta_{ij}\tilde{P}) - 2\left(\gamma_1 - f_{\mathrm{w1}}\gamma^* + \frac{C_3^*}{2}\Pi^{1/2}\right)k\bar{\mathbf{S}}_{ij} \\ & - C_6(G_{ij} - \frac{2}{3}\delta_{ij}G) - \frac{1}{3}\left(\frac{\partial}{\partial x_{\mathrm{m}}}\left(\nu\frac{\partial\overline{\mathbf{u}_i\mathbf{u}_k}}{\partial x_{\mathrm{m}}}\right)n_k n_j \right. \\ & \left. + \frac{\partial}{\partial x_{\mathrm{m}}}\left(\nu\frac{\partial\overline{\mathbf{u}_j\mathbf{u}_k}}{\partial x_{\mathrm{m}}}\right)n_k n_i\right) \\ & + \frac{1}{3}\frac{\partial}{\partial x_{\mathrm{m}}}\left(\nu\frac{\partial\overline{\mathbf{u}_k\mathbf{u}_p}}{\partial x_{\mathrm{m}}}\right)n_k n_p n_i n_j,\end{aligned} \tag{3c}$$

$$\varepsilon_{ij} = \frac{2}{3}(1-f_{\mathrm{w1}})\varepsilon\,\delta_{ij} + f_{\mathrm{w1}} \times \frac{\varepsilon}{k}\frac{\overline{\mathbf{u}_i\mathbf{u}_j} + \overline{\mathbf{u}_i\mathbf{u}_k}n_k n_j + \overline{\mathbf{u}_j\mathbf{u}_k}n_k n_i + n_i n_j\overline{\mathbf{u}_k\mathbf{u}_l}n_k n_l}{1 + 3\overline{\mathbf{u}_k\mathbf{u}_l}n_k n_l/2k}, \tag{3d}$$

where $C_{\mathrm{s}}, C_1, C_1^*, C_2$, α, α^*, β_1, γ_1, γ^* and C_3^* are specified in ref. [20] as 0.11, 3.4, 1.8, 4.2, 0.4125, -0.29, 0.2125, 0.0167, 0.065 and 1.3, respectively, while $\Pi = b_{ij}b_{ij}$, $b_{ij} = \overline{\mathbf{u}_i\mathbf{u}_j}/(2k) - (1/3)\,\delta_{ij}$ and $f_{\mathrm{w1}} = \exp[-(Re_t/200)^2]$ is introduced to account for the near-wall effects. Note that G_{ij} is exact and does not need modeling.

NEAR-WALL MODIFICATIONS OF THE DISSIPATION-RATE EQUATION FOR BUOYANT FLOWS

The extra term due to buoyancy in the ε-equation is proportional to $\varepsilon_{\theta i}$ in the $\overline{\mathbf{u}_i\theta}$ equation. For nonbuoyant flows, $\varepsilon_{\theta i}$ is zero away from the wall because there is no isotropic first-order tensor. However, buoyancy generates increased anisotropies and thus $\varepsilon_{\theta i}$ could be nonzero, even far from a wall. In view of this, there needs to be a buoyancy term in the high-Re ε-equation. Here, the model suggested by Bergstrom *et al.* [29] is adopted. Using a turbulent diffusion model similar to the one for $\overline{\mathbf{u}_i\mathbf{u}_j}$, the modeled ε-equation for buoyant flow is given by

$$\frac{D\varepsilon}{Dt} = \frac{\partial}{\partial x_k}\left(\nu\frac{\partial\varepsilon}{\partial x_k}\right) + \frac{\partial}{\partial x_i}\left(C_\varepsilon\frac{k}{\varepsilon}\overline{\mathbf{u}_i\mathbf{u}_j}\frac{\partial\varepsilon}{\partial x_j}\right) + C_{\varepsilon 1}\frac{\varepsilon}{k}\tilde{P} - C_{\varepsilon 2}\frac{\tilde{\varepsilon}}{k}\varepsilon + C_{\varepsilon 3}\frac{\varepsilon}{k}G + \xi, \tag{4}$$

where C_ε, $C_{\varepsilon 1}$, $C_{\varepsilon 2}$, $C_{\varepsilon 3}$ are assigned values 0.11, 1.5, 1.83, 1.5, respectively, and ξ is introduced to render equation (4) valid as a wall is approached.

The form of ξ is similar to that introduced in ref.

[20] for incompressible, nonbuoyant flows, but it needs modification to account for the buoyancy effects. Taking into account the buoyancy terms in the k-equation and adopting the approach proposed by Shima [30], the following compatibility condition is obtained for ε, or:

$$\frac{\partial \varepsilon}{\partial t} = -\nu \frac{\partial^2}{\partial x_k \partial x_k} + \nu \frac{\partial^2}{\partial x_k \partial x_k}\left(\frac{\partial^2 k}{\partial x_m \partial x_m}\right) - \nu \frac{\partial^2}{\partial x_k \partial x_k}\left(\overline{\mathbf{u}_l \mathbf{u}_m} \frac{\partial \bar{U}_l}{\partial x_m}\right) - \nu \frac{\partial^2}{\partial x_k \partial x_k}(\boldsymbol{g}_i \beta \overline{\mathbf{u}_i \theta}). \quad (5)$$

This condition stipulates that equation (4) should behave as equation (5) at the wall. Depending on the gravity vector, the buoyancy term in equation (5) can be nonzero as $y \to 0$; therefore, it must be accounted for in ξ. This buoyancy term is proportional to $\varepsilon_{\theta i}$. Furthermore, the buoyancy term in the exact ε-equation can be shown to be given by $G_\varepsilon = 2[\nu/(\nu+\alpha)]\boldsymbol{g}_i \beta \varepsilon_{\theta i}$. These analyses suggest that near-wall buoyancy effects in equation (4) can be accounted for by adopting G and G_ε in ξ to give

$$\xi = f_{w2}\left(-L\frac{\varepsilon}{k}\tilde{P} + M\frac{\tilde{\varepsilon}^2}{k} - N\frac{\varepsilon\tilde{\varepsilon}}{k} - C_{\varepsilon 3}\frac{\varepsilon}{k}G - 2\frac{\nu}{\nu+\alpha}\boldsymbol{g}_i \beta \varepsilon_{\theta i}\right), \quad (6)$$

where $L = 2.25$, $M = 0.5$ and $N = 0.57$ are as assumed in ref. [20] and the damping function in equation (6) is given in ref. [20] as $f_{w2} = \exp[-(Re_t/40)^2]$. Lai and So [28] have suggested a model term that reproduces the asymptotic behavior of $\varepsilon_{\theta i}$ near a wall. Their model is give by

$$\varepsilon_{\theta i} = \frac{1}{2}\left(1 + \frac{1}{Pr}\right)\frac{\varepsilon}{k}(\overline{\mathbf{u}_i \theta} + \overline{\mathbf{u}_k \theta} n_k n_i). \quad (7)$$

Therefore, the final proposal for ξ for buoyant flows is obtained by substituting equation (7) into equation (6).

EQUATIONS FOR THE TEMPERATURE VARIANCE AND ITS DISSIPATION RATE

There are no extra terms due to buoyancy in the equations for θ^2 and ε_θ. Consequently, the modeling of these equations can be accomplished just as in the nonbuoyant case. In other words, the modeled equations of So and Sommer [16] can be adopted without modification for buoyant flows. These equations are quoted here as

$$\frac{D\overline{\theta^2}}{Dt} = \frac{\partial}{\partial x_j}\left(\alpha \frac{\partial \overline{\theta^2}}{\partial x_j}\right) + \frac{\partial}{\partial x_k}\left(C_{\theta^2}\frac{k}{\varepsilon}\overline{\mathbf{u}_k \mathbf{u}_j}\frac{\partial \overline{\theta^2}}{\partial x_j}\right) - 2\overline{\mathbf{u}_j \theta}\frac{\partial \bar{\Theta}}{\partial x_j} - 2\varepsilon_\theta, \quad (8)$$

$$\frac{D\varepsilon_\theta}{Dt} = \frac{\partial}{\partial x_j}\left(\alpha \frac{\partial \varepsilon_\theta}{\partial x_j}\right) + \frac{\partial}{\partial x_k}\left(C_{\varepsilon\theta}\frac{k}{\varepsilon}\overline{\mathbf{u}_k \mathbf{u}_j}\frac{\partial \varepsilon_\theta}{\partial x_j}\right) + C_{d1}\frac{\varepsilon_\theta}{\overline{\theta^2}}P_\theta + C_{d2}\frac{\varepsilon}{k}P_\theta + C_{d3}\frac{\varepsilon_\theta}{k}\tilde{P} - C_{d4}\frac{\tilde{\varepsilon}_\theta}{\overline{\theta^2}}\varepsilon_\theta - C_{d5}\frac{\tilde{\varepsilon}}{k}\varepsilon_\theta + \xi_{\varepsilon_\theta}, \quad (9a)$$

$$\xi_{\varepsilon_\theta} = f_{w,\varepsilon_\theta}\left((C_{d4}-4)\frac{\tilde{\varepsilon}_\theta}{\overline{\theta^2}}\varepsilon_\theta + C_{d5}\frac{\tilde{\varepsilon}}{k}\varepsilon_\theta - \frac{\varepsilon_\theta^{*2}}{\overline{\theta^2}} + (2 - C_{d1} - PrC_{d2})\frac{\varepsilon_\theta}{\overline{\theta^2}}P_\theta^*\right), \quad (9b)$$

where ξ_{ε_θ} is the near-wall correction function, $f_{w,\varepsilon_\theta} = \exp[-(Re_t/80)^2]$ is a damping function introduced to account for near-wall viscous effects, and C_θ^2, C_{ε_θ}, C_{d1}, C_{d2}, C_{d3}, C_{d4}, C_{d5} are specified in ref. [16] as 0.11, 0.11, 1.80, 0, 0.72, 2.20, 0.80, respectively.

NEAR-WALL MODIFICATIONS OF THE HEAT-FLUX MODEL FOR BUOYANT FLOWS

It has been shown that predictions of $\overline{u\theta}$ using two-equation eddy thermal diffusivity models are greatly in error [19]. Consequently, an algebraic heat flux model based on the transport equations for $\overline{\theta^2}$ and ε_θ has been proposed and the predicted $\overline{\mathbf{u}\theta}$ is found to be in good agreement with the data, and with that given by a second-order model [9]. Since it is important to model $\overline{\mathbf{u}\theta}$ correctly in buoyant flows, the present approach extends the model of ref. [19] to account for buoyancy effects in near-wall flow calculations. There are two sources of extra terms due to gravity in the $\overline{\mathbf{u}_i\theta}$ equations. One is the explicit exact term, which does not require modeling in the equation. Another appears in the model proposed for the pressure-scrambling term. Using the high-Re version of the modeled $\overline{\mathbf{u}_i\theta}$ equation [21], the suggestions of Launder [23] for the buoyancy term and a fixed time scale [19], the $\overline{\mathbf{u}_i\theta}$ equation can be modeled to give

$$\frac{D\overline{\mathbf{u}_i\theta}}{Dt} = \frac{\partial}{\partial x_k}\left\{C_{s\theta}\frac{k}{\varepsilon}\left(\overline{\mathbf{u}_i\mathbf{u}_l}\frac{\partial \overline{\mathbf{u}_k\theta}}{\partial x_l} + \overline{\mathbf{u}_k\mathbf{u}_l}\frac{\partial \overline{\mathbf{u}_i\theta}}{\partial x_l}\right)\right\} - \overline{\mathbf{u}_i\mathbf{u}_j}\frac{\partial \bar{\Theta}}{\partial x_j} - \overline{\mathbf{u}_j\theta}\frac{\partial \bar{U}_i}{\partial x_j} - C_{1\theta}\sqrt{\frac{\varepsilon\varepsilon_\theta}{k\overline{\theta^2}}}\overline{\mathbf{u}_i\theta} + C_{2\theta}\overline{\mathbf{u}_j\theta}\frac{\partial \bar{U}_i}{\partial x_j} + C_{3\theta}\boldsymbol{g}_i\beta\overline{\theta^2} - \boldsymbol{g}_i\beta\overline{\theta^2}, \quad (10)$$

where $C_{s\theta} = 0.11$ and $C_{1\theta} = 3.28$ are suggested. Note that the dissipation of the turbulent heat fluxes is set to zero for the flows considered here and the suggestion $C_{3\theta} = C_{2\theta} = 0.4$ [23] is adopted. The reduction of equation (10) into an algebraic equation for $\overline{\mathbf{u}_i\theta}$ follows naturally from the assumption of local equilibrium of turbulence. Thus obtained, the algebraic

equations are not explicit in terms of $\overline{\mathbf{u}_i\theta}$ and numerical instability could result from matrix inversion for certain mean flow conditions [18]. So and Sommer [19] suggest further simplification by replacing all Reynolds flux terms on the right hand side of the implicit algebraic equations with gradient transport models, thus rendering the algebraic equations explicit. A detailed discussion of this is given in ref. [19]. After much algebra, the $\overline{\mathbf{u}_i\theta}$ equation for buoyant flows can be written as

$$-\overline{\mathbf{u}_i\theta} = \alpha_t \frac{\partial\bar{\Theta}}{\partial x_i} - \frac{1}{C_{1\theta}}\sqrt{\frac{k}{\varepsilon}\frac{\overline{\theta^2}}{\varepsilon_\theta}}((2\nu_t + (1-C_{2\theta})\alpha_t)\bar{\mathbf{S}}_{ik} + (1-C_{2\theta})\alpha_t\bar{\mathbf{W}}_{ik})\frac{\partial\bar{\Theta}}{\partial x_k} + \frac{(1-C_{2\theta})}{C_{1\theta}}\sqrt{\frac{k}{\varepsilon}\frac{\overline{\theta^2}}{\varepsilon_\theta}}\mathbf{g}_i\beta\overline{\theta^2}. \quad (11)$$

The only difference between equation (11) and that derived in ref. [19] is the buoyancy term. Since this term is of order y^4, the same asymptotic behavior as in the nonbuoyant case can be obtained if the near-wall model for the eddy thermal diffusivity $\alpha_t = C_\lambda f_\lambda k(k\overline{\theta^2}/\varepsilon\varepsilon_\theta)^{1/2}$ and the eddy viscosity $\nu_t = C_\mu f_\mu k^2/\varepsilon$ for nonbuoyant flows are adopted. According to ref. [16], the constants and damping functions are given by $C_\mu = 0.096$, $C_\lambda = 0.095$, $f_\lambda = f_{\lambda 1} + [1-f_{\lambda 1}](C_{\lambda 1}/Re_t^{1/4})$, $f_{\lambda 1} = [1-\exp(-y^+/A^+)]^2$, $C_{\lambda 1} = 0.4/Pr^{1/4}$ for $Pr < 0.1$ and $C_{\lambda 1} = 0.07/Pr$ for $Pr \geqslant 0.1$, $A^+ = 10/Pr$ for $Pr < 0.25$ and $A^+ = 39/Pr^{1/16}$ for $Pr \geqslant 0.25$, and $f_\mu = [1+3.45Re_t^{1/2}]\tanh(y^+/115)$.

FULLY-DEVELOPED HORIZONTAL CHANNEL FLOWS WITH VERTICAL STRATIFICATION

In the fully developed region of a horizontal plane channel flow with vertical stratification, there are no buoyancy terms in the $\bar{U}$ equation. Consequently, buoyancy acts on the turbulence field alone and only a structural effect is present. In view of this, the performance of the present model can be assessed against this flow. Experimental data for such a flow have been collected by Petukhov *et al.* [31, 32] and summarized by Petukhov and Polyakov [22]. They studied the flow in a horizontal channel with an aspect ratio of 1/45. In order to obtain a stable or unstable stratification, the top or bottom wall, respectively, was heated while the opposite wall was adiabatic. Likewise the side walls were adiabatic. Measurements were taken in the central region of about 30–40% of the channel width where the flow was essentially two-dimensional with no secondary cells observed [31]. Under fully developed conditions, the flow becomes asymmetric with respect to the centerline of the channel and the wall shear stresses at the hot and cold walls are quite different. Integrating the $\bar{U}$ equation gives the following:

$$\frac{dU^+}{dy^+} = \left(\frac{dU^+}{dy^+}\right)_h - \frac{y^+}{Re_\tau} + \overline{uv}^+, \quad (12)$$

where subscript h indicates wall condition. For this flow, Petukhov and Polyakov [22] derived an estimate for Gq_{th}, which is defined as the Gq in which Nu or St changes by 1% from its value at neutral stratification. Their estimate can be written as

$$Gq_{th} = 8.07\times 10^{-4} Pr^{1.12} Re^{2.75}. \quad (13)$$

The driving force for this flow is the streamwise pressure gradient, which is constant in both the streamwise and cross-stream directions in the fully developed region. In carrying out this calculation, it is most appropriate to match the pressure gradient, which can be related to Re_τ based on $\bar{u}_\tau$, with experimental data. The second important parameter for buoyant flows is Gq. It can be seen from equation (13) that the onset of noticeable buoyancy effects depend on Re. Therefore, for the present calculations, it is decided to match Gq/Gq_{th} rather than Gq itself. This allows a meaningful comparison of the results at different Re. Re_τ is estimated from $2Re_\tau = Re\sqrt{\bar{C}_f/2}$, where $\bar{C}_f$ is calculated from a correlation given in ref. [22] as

$$\frac{\bar{C}_f}{C_{f,0}} = 1 \pm 178.38\frac{Gq}{PrRe^{2.75}} \quad (14)$$

and $C_{f,0}$ is taken as an average value of three established correlations [22]. The calculated $\bar{C}_f$ and Nu are compared to the values deduced from equation (14) and the following correlation for Nu [32]:

$$\frac{Nu}{Nu_0} = 1 \pm 0.01\frac{Gq}{Gq_{th}}. \quad (15)$$

In equations (14) and (15), the plus and minus signs correspond to unstable and stable stratification, respectively, while Nu_0 is defined for neutral stratification as

$$Nu_0 = \frac{RePr\bar{C}_f}{2+(900/Re)+5.4(\bar{C}_f/2)^{1/2}(Pr^{2/3}-1)}. \quad (16)$$

Calculations are performed using the present model and a simple k-ε model composed of equation (4), a k-equation given by one half the trace of equation (3a), $-\overline{uv} = \nu_t(\partial\bar{U}/\partial y)$, $-\overline{v\theta} = (\nu_t/Pr_t)(\partial\bar{\Theta}/\partial y)$, $\nu_t = C_\mu f_\mu k^2/\varepsilon$ and $Pr_t = 0.9$. This simple model differs drastically from the present model, in that it only solves two modeled equations and assumes isotropic turbulence. The wall boundary conditions are the usual no slip condition for the velocity and turbulence field, specified constant wall temperature or wall heat flux for the mean thermal field, zero temperature variance at the wall, and finite ε_w and $\varepsilon_{\theta,w}$. The most important quantities to compare are $\bar{C}_f$ and Nu because of their practical importance and the availability of empirical correlations, (14) and (15), derived from experiments.

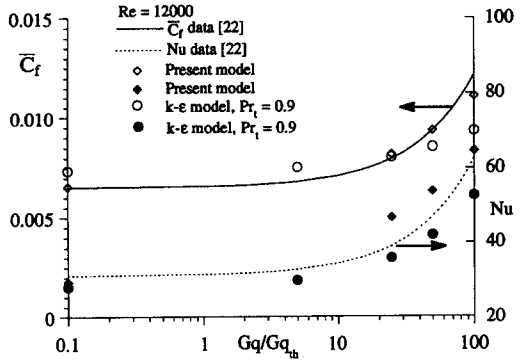

Fig. 1. Comparison of calculated $\bar{C}_f$ and Nu with data under unstable stratification.

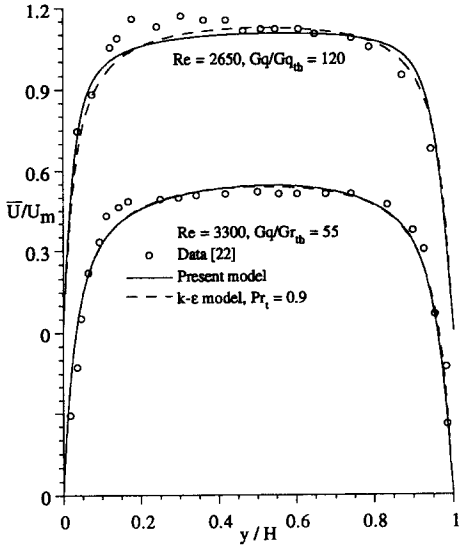

Fig. 2. Linear plot of mean velocity under unstable stratification.

Any model calculation should at least be able to reproduce the measured trends of these parameters, even if some of the flow details are not captured correctly.

Equations (14) and (15) show that, under unstable stratification, both $\bar{C}_f$ and Nu increase with increasing buoyancy, because the additional buoyancy terms in the turbulence equations are generation terms and thus enhance turbulence. The process can be understood if a fluid parcel transported by turbulent motion is considered. Under unstable stratification, i.e. heating from below, a parcel moving away from the bottom wall will move into a colder, heavier fluid and buoyancy force tends to push the parcel further than it would have in an isothermal flow. Conversely, a parcel moving towards the heated bottom wall will encounter warmer, lighter fluid and drops further towards the wall than in the absence of buoyancy. A comparison of the calculated $\bar{C}_f$ and Nu with equations (14) and (15) shows that both the present model and the k-ε model are in reasonable agreement with the data (Fig. 1). The present model gives slightly better results for $\bar{C}_f$, particularly at low Re with strong buoyancy effects, while the k-ε model predicts Nu more accurately at low Re. However, at higher Re, such as $Re = 12\,000$, the present results are in better agreement with data for both $\bar{C}_f$ and Nu (Fig. 1). The present model does a fair job in reproducing the increase of $\bar{C}_f$ with increasing Gq/Gq_{th} and its predictions are in agreement with data up to $Gq/Gq_{th} \approx 100$, while the k-ε model results deviate from data around $Gq/Gq_{th} = 30$. On the other hand, the calculated Nu is in good agreement with the data for both models.

Linear plots of the velocity profiles at $Re = 3300$, $Gq/Gq_{th} = 55$ and $Re = 2650$, $Gq/Gq_{th} = 120$ are shown in Fig. 2. The calculated $\bar{C}_f$ and Nu by the present model for the $Re = 3300$ case are 13.73×10^{-3} and 24.39, respectively, while they are 19.81×10^{-3} and 26.90 for the $Re = 2650$ case. These results are very comparable with 13.41×10^{-3} and 17.72 for the $Re = 3300$ case, and 19.63×10^{-3} and 20.15 for the $Re = 2650$ case obtained by Petukhov *et al.* [31]. On the other hand, the k-ε model with $Pr_t = 0.9$ yields the following pair of values for the two cases: 12.99×10^{-3} and 16.08, 15.33×10^{-3} and 17.61. At $Gq/Gq_{th} = 55$, both the present model and the k-ε model yield nearly identical results, which are in good agreement with the data. Consistent with the calculated $\bar{C}_f$ given above, the present model predicts a fuller velocity profile than the k-ε model at $Gq/Gq_{th} = 120$. Both models predict the maximum velocity to be located in the upper half of the channel, closer to the adiabatic wall. The trend is opposite to that shown by the measurements, which have a much more marked maximum in the lower half (Fig. 2). This difference is quite significant and needs clarification.

According to equation (12), the velocity gradient is equal to the difference between $(dU^+/dy^+)_h - y^+/Re_\tau$ and $-\overline{uv}^+$. A plot of the various terms in equation (12) is shown in Fig. 3. It is obvious that the velocity gradient is very small near the centerline of the channel. Furthermore, the difference between the lines corresponding to $(dU^+/dy^+)_h - y^+/Re_\tau$ and $-\overline{uv}^+$ is small over a large portion of the channel. Thus, a small disturbance could move the location of the maximum velocity, i.e. the point where the velocity gradient is

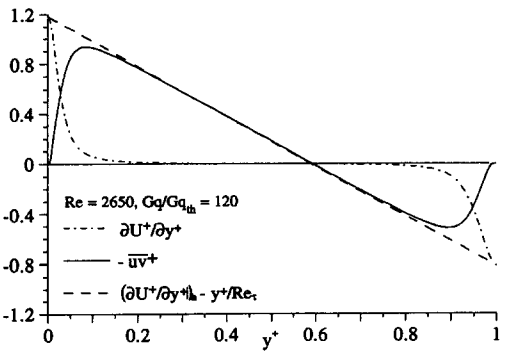

Fig. 3. A plot of the shear stress and derivative of mean velocity.

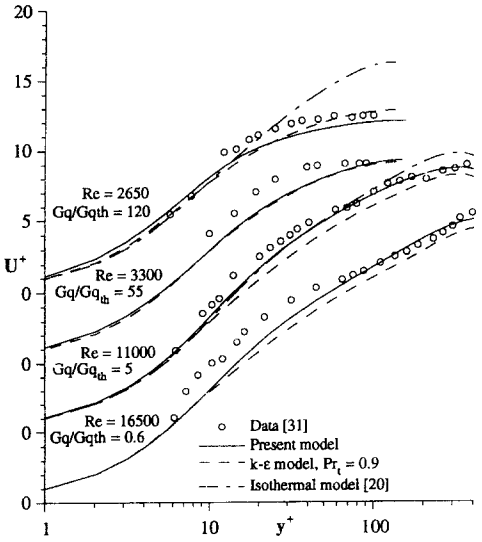

Fig. 4. Log plot of mean velocity under unstable stratification.

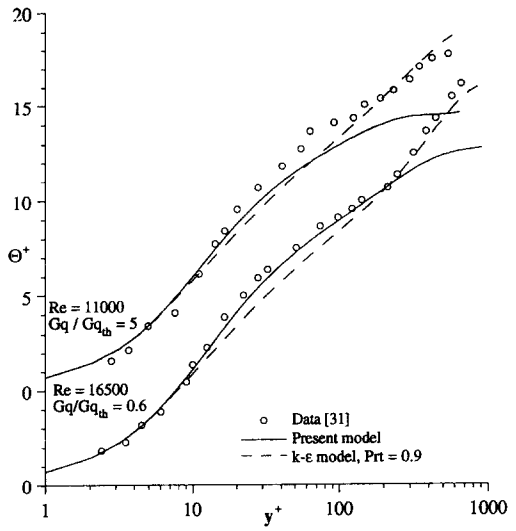

Fig. 5. Log plot of mean temperature under unstable stratification.

zero, from one half of the channel to the other. It is conceivable that a weak secondary flow in the experiments could provide the necessary potential to effect the switch. Such a secondary flow in this test case could arise from a thermal instability due to the heating from below. Furthermore, the side walls may not be perfectly adiabatic, thus giving rise to a secondary motion due to the wall heat flux. Both these effects could lead to the formation of longitudinal vortices. There could also be an interaction between the secondary flow due to corner effects with buoyancy. In view of this, there is a variety of possible sources for secondary cells that, in spite of being very weak, could still be sufficient to provide the necessary potential to drive the velocity maximum from one half of the channel to the other. This analysis casts doubts on the measured location of the velocity maximum in any two-dimensional buoyant flow experiments. At the very least, this study shows that the location of the maximum velocity is a very sensitive quantity to measure and predict.

The mean velocities are further compared in logarithmic plots which show that the present results are in better agreement with data for high Re and weak buoyancy as well as for low Re and strong buoyancy (Fig. 4). In particular, the shape of the velocity profile at $Re = 2650$, $Gq/Gq_{th} = 120$ is correctly predicted using the present model. In two cases, a comparison is also made with the model calculations of So *et al.* [20] for isothermal flows. It can be seen that there is a layer near the wall where the buoyant and isothermal results are essentially identical. Petukhov and Polyakov [22] call this region the dynamic sublayer. For the case of weak buoyancy and high Re ($Re = 11\,000, Gq/Gq_{th} = 5$), the dynamic sublayer extends beyond the viscous sublayer into the buffer layer, while for stronger buoyancy and lower Re ($Re = 2650, Gq/Gq_{th} = 120$), the dynamic sublayer, according to model predictions, is about equal to the viscous sublayer. This verifies the assumption that, near the wall, the buoyancy effects are negligible compared to viscous effects.

The results of $\bar{\Theta}$ for two cases where $Re = 16\,500$, $Gq/Gq_{th} = 0.6$ and $Re = 11\,000$, $Gq/Gq_{th} = 5.0$ are shown in Fig. 5. The present results are in better agreement with the data in almost the entire lower half of the channel, while the k-ε model yields a more correct prediction in the upper half. Since buoyancy force influences the turbulence mainly through $\overline{v\theta}$, which is largest in the lower half of the channel and smallest near the adiabatic wall, it is more important to have a good agreement of the calculated temperature field with the data in the lower half of the channel. This explains why the velocity profile is in better agreement with the present model than with the k-ε model, even though there are significant discrepancies between the calculated and measured $\bar{\Theta}$ in the upper half of the channel. On the other hand, these discrepancies could affect the calculated Nu. This comparison, therefore, provides some insight as to why the simpler k-ε model gives, in some cases, better results for Nu. Finally, sample comparisons of u_{rms} and θ_{rms} with measurements are shown in Figs. 6 and 7. In the u_{rms} case, the agreement with data is reasonable. On the other hand, it can be seen that θ_{rms} increases with increasing unstable stratification and is consistent with data. However, the quantitative agreement is poor.

DEVELOPING TURBULENT FLOW IN A HEATED VERTICAL PIPE

Mixed convection in a vertical pipe has been studied by numerous researchers. The vast majority of the

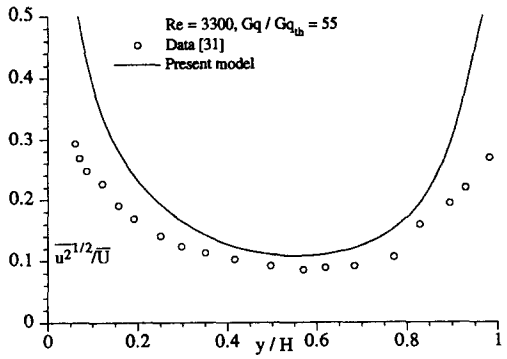

Fig. 6. Comparison of streamwise turbulence intensity with data under unstable stratification.

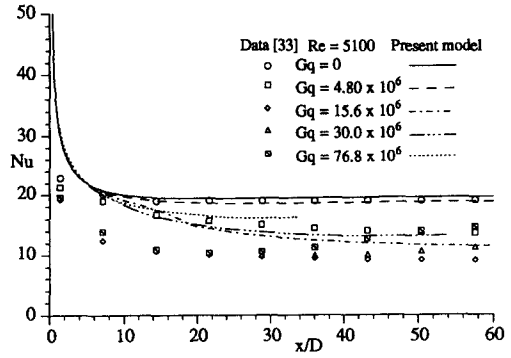

Fig. 8. Comparison of calculated Nu with data under stable stratification.

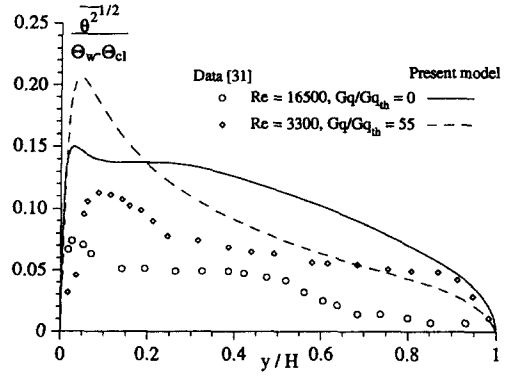

Fig. 7. Comparison of temperature fluctuation with data under unstable stratification.

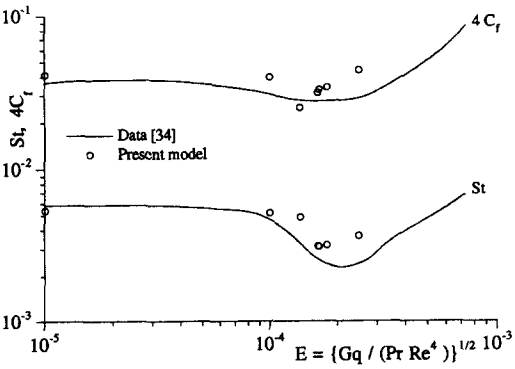

Fig. 9. Comparison of calculated C_f and St with data under stable stratification.

experimental investigations are for the case of a stable stratification, i.e. upward flow with a heated wall. Among these studies, the experiments of Polyakov and Shindin [33] are of particular interest. There are not as many investigations on flow with an unstable stratification, i.e. downward flow in a heated pipe. However, the summary of research [22] could be mentioned. Since most of these studies do not provide accurate measurements of turbulence quantities, comparisons can only be made with C_f, St and possibly $\bar{U}$ and $\bar{\Theta}$. The calculations of the various cases were carried out in much the same way as for the thermal entrance region calculations for nonbuoyant flow in a pipe [19], i.e. starting with a fully developed velocity profile for isothermal flow, a uniform inlet temperature and the thermal turbulence statistics as described in ref. [19]. With the exception of the mean wall thermal boundary conditions, other conditions similar to those invoked for the horizontal channel flow with vertical stratification are also adopted. For the Polyakov and Shindin [33] flow cases, a constant wall heat flux is specified just as in the experiments.

A comparison of the calculated and measured Nu variations with x/D is shown in Fig. 8. On first sight, both the measurements and calculations paint a rather confusing picture. With increasing Gq, Nu first decreases to values smaller than the nonbuoyant case. However, as Gq increases, Nu at a given location starts to increase. This behavior can be explained by the interplay between the structural and external effects of buoyancy. When buoyancy is small, the structural effect, i.e. the direct influence of buoyancy on the turbulence field, is more important. As a result of stable stratification, the turbulence intensity is decreased and, consequently, Nu decreases. With increasing Gq, a point is reached where the structural effects are no longer dominant. Rather, the external effect, i.e. the direct influence of buoyancy on the mean field, becomes more important. At this point the turbulence intensities become very small, therefore, a further decrease in intensities no longer exerts a major influence. Instead, the behavior resembles the laminar case in which Nu increases monotonically with increasing buoyancy influence. This behavior is confirmed by the plots of St and C_f shown in Fig. 9 as a function of the buoyancy parameter, $E = [Gq/Re^4Pr]^{1/2}$, which appears naturally in the governing equations if they are nondimensionalized consistently [34]. The calculated results shown in Fig. 9 correspond to the cases where the C_f and St were determined at $x/D = 53$ for the experiments of Polyakov and Shindin [33], and at $x/D = 100$ with reported mean flow measurements. The comparison at different x/D is justified because the calculated Nu changes very little beyond $x/D = 40$.

It can be seen from both Figs. 8 and 9 that the

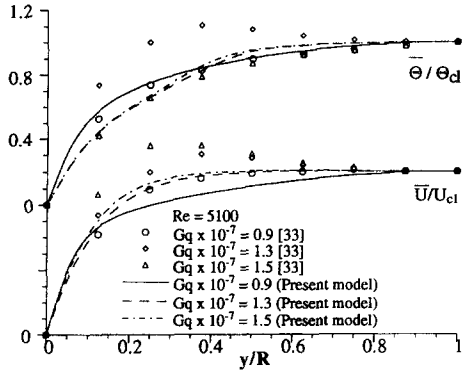

Fig. 10. Comparison of calculated U and Θ with data under stable stratification.

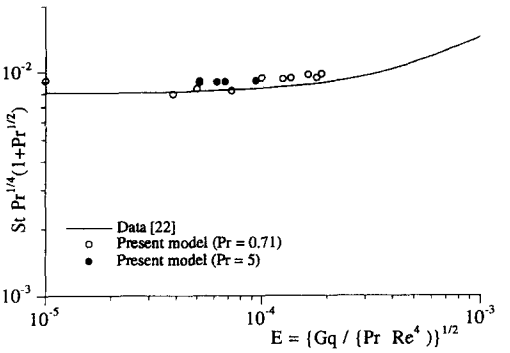

Fig. 11. Comparison of $StPr$ correlation with data under stable stratification.

present model essentially reproduces the correct behavior of Nu, St and C_f. There are, however, some discrepancies between the calculations and measurements. The point at which the calculated integral parameters deviate from their nonbuoyant value occurs at too high a value of E or Gq. The magnitude of the decrease in St is under-predicted, while the change of C_f is over-estimated. A further discrepancy is the behavior of Nu with increasing streamwise distance at high Gq. For the two highest Gq, the data show that Nu is increasing beyond $x/D = 35$. The calculations fail to reproduce this trend. In fact, it is not possible to obtain results beyond this point for the highest Gq. The reason for this can be explained by examining the behaviour of the measurements. The Nu increase beyond $x/D = 35$ is due to the fact that the flow becomes more and more like a laminar flow, for which Nu is higher at this Gq. This means that the turbulence has been substantially suppressed. When the calculations are examined at the last downstream locations where the results are available, it could be seen that in the immediate near-wall region, $\overline{\mathbf{u}_i\mathbf{u}_j}$ are essentially zero. In other words, the production due to mean shear is no longer sufficient to sustain the turbulence against destruction due to dissipation and buoyancy. Since the present model is not designed to handle reverse transition, it is not possible to calculate beyond this point.

The discrepancy in the integral parameters can be correlated to discrepancies in the mean flow profiles. Figure 10 compares the calculated $\bar{U}$ and $\bar{\Theta}$ to the measurements of Polyakov and Shindin [33]. Again, the comparisons are made at $x/D = 53$. The predicted trend is correct, i.e. the velocity profile becomes fuller with increasing buoyancy. However, the experimental results show a rather marked maximum of $\bar{U}$ at $y/R \approx 0.3$ for the higher Grashof numbers ($Gq = 1.3 \times 10^7, Gq = 1.5 \times 10^7$). On the other hand, the calculations show a very weak maximum at best. It should be noted that, for even higher Gq, the maximum observed in the experiments becomes weaker [33]. This behavior of $\bar{U}$ is very much in line with the observed St and C_f. The calculated temperature profiles are in reasonable agreement with the data for the cases at $Gq = 9 \times 10^6$ and $Gq = 1.5 \times 10^7$, but in poor agreement at $Gq = 1.3 \times 10^7$. This poor agreement cannot be explained easily because the measurements are not very consistent with increasing Gq, while the predictions are.

There is much less experimental work on flows with unstable stratification. Therefore, comparison between model calculations and data are limited to integral parameters only. A comparison of the calculated St with the data of Petukhov and Polyakov [22] can be made. They found that, for $0.6 \leqslant Pr \leqslant 20$, the parameter $StPr^{1/4}(1+St^{1/2})$ collapses to a single curve as a function of E, irrespective of the value of Pr. To test the ability of the present model to capture this feature, several calculations are carried out at $Pr = 0.71$ and 5. The calculated $StPr^{1/4}(1+St^{1/2})$ is compared with a curve fit through the data presented by Petukhov and Polyakov [22] in Fig. 11. The $StPr^{1/4}(1+St^{1/2})$ results collapse into a single correlation for the two Pr considered. Furthermore, the predictions are in good agreement with the curve fit, and the discrepancy is well within the scatter of experimental data shown by Petukhov and Polyakov [22]. Therefore, this comparison shows that the present model is capable of capturing the basic physics of convective heat transfer in a vertical pipe under unstable stratification.

CONCLUSIONS

A turbulence model has been proposed for near-wall flows with buoyancy influence. The model is based on the transport equations for $\overline{\mathbf{u}_i\mathbf{u}_j}$, ε, $\overline{\theta^2}$ and ε_θ. Additional terms, both exact and model terms, have been introduced compared to the nonbuoyant flow model in the $\overline{\mathbf{u}_i\mathbf{u}_j}$ and ε equations and, where appropriate, near-wall corrections are introduced in order to obtain the proper asymptotic behavior as the wall is approached. The turbulent heat fluxes are calculated using an explicit heat flux model with extra terms due to buoyancy added. A near-wall damping function

identical to its nonbuoyant counterpart is used to enforce the correct asymptotic behavior for $-\overline{v\theta}$.

The model is validated against two different types of internal flow. One is a fully developed horizontal plane channel flow with vertical stratification, while the other is the flow in a heated vertical pipe. For both geometries, calculations are performed for stable and unstable stratifications. In general, the model results for integral quantities are in good agreement with data and reflect the proper physics. There are some discrepancies between the data and calculations for mean flow and turbulence quantities. However, in view of the complexity of the flows studied, these discrepancies are not too severe. The model correctly predicts the trend of enhanced turbulence with increasingly unstable stratification and the reduction of the turbulence intensity when the stratification is stable. The nonbuoyant version of the model has been applied to a wide variety of incompressible flows with and without heat transfer and good correlations are obtained [16, 19, 20]. Together these results show that the present model can be applied to buoyant as well as nonbuoyant incompressible near-wall flows.

Acknowledgements—The authors wish to acknowledge support given them by NASA Langley Research Center, Hampton, Virginia, under grant no. NAG-1-1080, which was monitored by Dr T. B. Gatski.

REFERENCES

1. V. C. Patel, W. Rodi and G. Scheuerer, Turbulence models for near-wall and low-Reynolds number flows, *AIAA J.* **23,** 1308–1319 (1985).
2. R. M. C. So, Y. G. Lai, H. S. Zhang and B. C. Hwang, Second-order near-wall turbulence closures: a review, *AIAA J.* **29,** 1819–1835 (1991).
3. H. B. Mason and R. A. Seban, Numerical predictions for turbulent free convection from vertical surfaces, *Int. J. Heat Mass Transfer* **17,** 1329–1336 (1974).
4. S. J. Lin and S. W. Churchill, Turbulent free convection from a vertical isothermal pipe, *Numer. Heat Transfer* **1,** 129–145 (1978).
5. N. C. Markatos and K. A. Pericleous, Laminar and turbulent natural convection in an enclosed cavity, *Int. J. Heat Mass Transfer* **27,** 755–772 (1984).
6. W. M. Yan and T. F. Lin, Heat transfer in buoyancy-driven flows with the simultaneous presence of laminar transitional and turbulent flow regimes, *Wärme-Stoffübertragung* **24,** 125–132 (1989).
7. W. M. Yan and T. F. Lin, Theoretical and experimental study of natural convection pipe flows at high Rayleigh number, *Int. J. Heat Mass Transfer* **34,** 291–303 (1991).
8. W. M. To and J. A. C. Humphrey, Numerical simulation of buoyant turbulent flow—I. Free convection along a heated, vertical, flat plate, *Int. J. Heat Mass Transfer* **29,** 573–592 (1986).
9. A. Shabbir and D. B. Taulbee, Evaluation of turbulence models for predicting buoyant flows, *J. Heat Transfer* **112,** 945–951 (1990).
10. R. Morel, A. Laassibi, E. Alcaraz, R. Zegadi, G. Brun and D. Jeandel, Validation of a k-ε model based on experimental results in a thermally stable stratified turbulent boundary layer, *Int. J. Heat Mass Transfer* **35,** 2717–2724 (1992).
11. M. S. Hossain and W. Rodi, Mathematical modelling of vertical mixing in stratified channel flow, *Proceedings of the Second International Symposium on Stratified Flows*, Trondheim, Norway, Vol. 1, pp. 280–290 (1980).
12. M. Ljuboja and W. Rodi, Prediction of horizontal and vertical turbulent buoyant wall jets, *J. Heat Transfer* **103,** 343–349 (1981).
13. M. K. Chung and H. J. Sung, Four-equation turbulence model for prediction of the turbulent boundary layer affected by buoyancy force over a flat plate, *Int. J. Heat Mass Transfer* **27,** 2387–2395 (1984).
14. E. Uspuras and P. Poskas, Numerical analysis of turbulent transport in combined (forced and free) convection in vertical channels, *Heat Transfer—Sov. Res.* **23,** 751–774 (1991).
15. T. Cebeci and P. Bradshaw, *Physical and Computational Aspects of Convective Heat Transfer*, pp. 13, 19–31, 150–151. Springer, New York (1984).
16. R. M. C. So and T. P. Sommer, A near-wall eddy conductivity model for fluids with different Prandtl numbers, *J. Heat Transfer* **116,** 844–854 (1994).
17. T. P. Sommer, R. M. C. So and H. S. Zhang, Heat transfer modeling and the assumption of zero wall temperature fluctuations, *J. Heat Transfer* **116,** 855–863 (1994).
18. T. B. Gatski and C. G. Speziale, On explicit algebraic stress models for complex turbulent flows, *J. Fluid Mech.* **254,** 59–78 (1993).
19. R. M. C. So and T. P. Sommer, An explicit algebraic heat-flux model for the temperature field, *Int. J. Heat Mass Transfer* **39,** 455–465 (1996).
20. R. M. C. So, H. Aksoy, T. P. Sommer and S. P. Yuan, Development of a near-wall Reynolds-stress closure based on the SSG model for the pressure strain, NASA Contractor Report 4618 (1994).
21. C. G. Speziale, S. Sarkar and T. B. Gatski, Modeling the pressure–strain correlation of turbulence: an invariant dynamical systems approach, *J. Fluid Mech.* **227,** 245–272 (1991).
22. B. S. Petukhov and A. E. Polyakov, *Heat Transfer in Turbulent Mixed Convection*, pp. 38, 41, 115–131, 147–182. Hemisphere, New York (1988).
23. B. E. Launder, Heat and mass transport. In *Topics in Physics, Vol. 12 Turbulence* (Edited by P. Bradshaw), pp. 231–287. Springer, New York (1978).
24. B. Gebhart, J. Jaluria, R. L. Mahajan and B. Sammakia, *Buoyancy-Induced Flows and Transport*, pp. 28–30. Hemisphere, New York (1988).
25. K. Hanjalic and B. E. Launder, Contribution towards a Reynolds-stress closure for low-Reynolds-number turbulence, *J. Fluid Mech.* **74,** 593–610 (1976).
26. A. N. Kolmogorov, The local structure of turbulence in an incompressible viscous fluid for very large Reynolds numbers, *Comptes Rendus Acad. Sci.* U.S.S.R. **30,** 301–305 (1941) [Translation, *Turbulence, Classic Papers on Statistical Theory* (Edited by S. K. Friedlander and L. Topper). Interscience, New York (1961).]
27. Y. G. Lai and R. M. C. So, On near-wall turbulent flow modeling, *J. Fluid Mech.* **221,** 641–673 (1990).
28. Y. G. Lai and R. M. C. So, Near-wall modeling of turbulent heat fluxes, *Int. J. Heat Mass Transfer* **33,** 1429–1440 (1990).
29. D. J. Bergstrom, G. D. Stubley and A. B. Strong, Numerical prediction of countergradient thermal transport in a turbulent plume, *ASHRAE Trans. Res.* **99,** 422–429 (1993).
30. N. Shima, A Reynolds-stress model for near-wall and low-Reynolds-number regions, *J. Fluids Engng* **110,** 38–44 (1988).
31. B. S. Petukhov, A. F. Polyakov and Y. V. Tsypulev, Peculiarities of non-isothermal turbulent flow in hori-

zontal plane channels at low Reynolds numbers and under significant buoyancy forces. In *Turbulent Shear Flows*, Vol. 2, pp. 158–167. Springer, Heidelberg (1980).
32. B. S. Petukhov, A. F. Polyakov and Y. V. Tsypulev, Turbulent momentum and heat transfer in thermally-stratified flows, *Heat Transfer—Sov. Res.* **13,** 56–68 (1981).
33. A. F. Polakov and S. A. Shindin, Development of turbulent heat transfer over the length of vertical tubes in the presence of mixed air convection, *Int. J. Heat Mass Transfer* **31,** 987–992 (1988).
34. A. F. Polyakov, Turbulent forced flow and heat transfer in vertical channels under the conditions of free convection, *J. Engng Phys.* **35,** 801–811 (1978).